Mapping the site-specific potential energy landscape for chemisorbed and physisorbed aromatic molecules on the Si(1 1 1)-7 × 7 surface by time-lapse STM

2015 J. Phys.: Condens. Matter 27 054003

(http://iopscience.iop.org/0953-8984/27/5/054003)

OPEN ACCESS
IOP Publishing
Journal of Physics: Condensed Matter
J. Phys.: Condens. Matter **27** (2015) 054003 (7pp)
doi:10.1088/0953-8984/27/5/054003

Mapping the site-specific potential energy landscape for chemisorbed and physisorbed aromatic molecules on the Si(1 1 1)-7×7 surface by time-lapse STM

D Lock[1], S Sakulsermsuk[2], R E Palmer[2] and P A Sloan[1]

[1] Department of Physics, University of Bath, North East Somerset BA2 7AY, UK
[2] Nanoscale Physics Research Laboratory, School of Physics and Astronomy, University of Birmingham, West Midlands B15 2TT, UK

E-mail: p.sloan@bath.ac.uk

Received 28 July 2014, revised 26 September 2014
Accepted for publication 29 September 2014
Published 21 November 2014

Abstract

We present a scanning tunnelling microscope study of site-specific thermal displacement (desorption or diffusion) of benzene, toluene, and chlorobenzene molecules on the Si(1 1 1)-7×7 surface. Through time-lapse STM imaging and automated image analysis we probe both the chemisorbed and the physisorbed states of these molecules. For the chemisorption to physisorption transition there are distinct site-specific variations in the measured rates, however their kinetic origin is ambiguous. There is also significant variation in the competing rates out of the physisorbed state into chemisorption at the various surface sites, which we attribute to differences in site-specific Arrhenius pre-factors. A prediction of the outcome of the competing rates and pre-factors for benzene over three hours matches experiment.

Keywords: scanning tunnelling microscopy, Si(1 1 1)-7×7, benzene, toluene, chlorobenzene, pre-cursor, chemisorption

(Some figures may appear in colour only in the online journal)

1. Introduction

Small organic molecules chemisorbed on a semiconductor surface are predicted to form a possible route to a truly molecular-scale nanotechnology [1–4]. Towards this aim there has been a focus on using the tip of the scanning tunnelling microscope (STM) to induce atomic and molecular manipulation to build designer nano-structures with many striking results [5–7]. Underpinning these works are the ground-state properties of the target atoms and molecules. To gain a full understanding of atomic and molecular manipulation therefore requires knowledge of the underlying ground-state properties of the target systems. Unless the molecule/surface system is essentially ideal, there will be more than one possible binding site and binding configuration. Therefore surface-science techniques that probe large areas are inherently limited to averaging over all the possible binding sites. To enable a true measurement of the properties of a particular molecule/surface configuration requires atomic resolution. The STM is therefore an ideal tool to not only perform atomic manipulation but to probe the underlying ground-state properties. Furthermore, accurate experimental data on complex systems provides a challenging benchmark to test theoretical models of the potential energy surface (PES) [8–10].

In order to measure the ground-state properties there must be some alteration of the molecule/surface system within the time-scale of the measurement. For a thermally induced process this is governed by the Arrhenius equation, $R = A\exp(-E/kT)$ where A is related to the properties of the

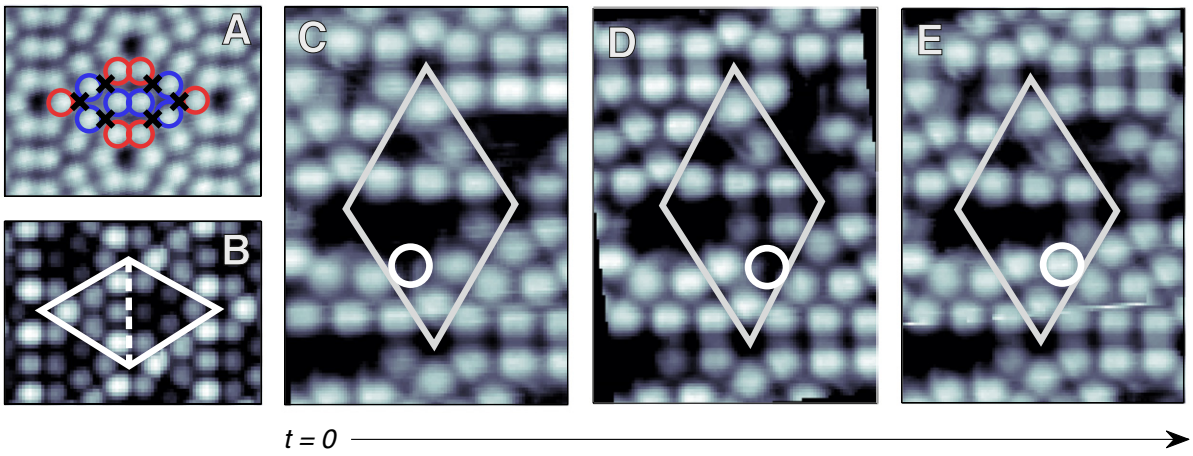

Figure 1. (*a*, *b*) 6 × 7 nm STM images recorded at +1 V (*a*) and −1 V (*b*), 100 pA. At negative bias, the faulted half (left triangle) is brighter than the unfaulted (right triangle). Red circles: corner adatoms, adjacent to the dark corner hole. Blue circles: middle adatoms. Crosses: rest atoms. (*c*)–(*e*) STM images (5.1 × 7.0 nm, +1 V, 100 pA) taken 3 min apart. One rhombohedral 7 × 7 unit cell with an initial coverage of 4 toluene molecules is highlighted, (*c*). A toluene molecule replaces a bright adatom in STM, seen as a dark spot. The circled molecule moves to a neighbouring adatom site (*d*) and desorbs (*e*).

transition state, E the energy barrier to the transition state, k Boltzmann's constant and T the temperature. If the STM tip is located above a particular site and the tunnel current recorded as a function of time, the STM can have a time resolution from seconds down to μs [11]. However, the mere presence of the STM tip can alter the thermally induced molecular dynamics. For example, we have recently shown that the thermally induced binding site switching of polychlorinatedbiphenyl (PCB) on Si(1 1 1)-7×7 is subtly influenced by the presence of the STM tip [12].

To reduce the possible influence of the STM tip here we use time-lapse STM scanning. Unlike normal STM imaging where images are taken one after another, here we introduce a sizeable time delay between images. Sequential images are typically taken over 12 min intervals, and each image (60 nm × 60 nm) takes ∼3 min to complete, therefore each atomic site (0.5 nm × 0.5 nm) will only experience the presence of an STM tip for ∼10 ms every 10 min. Non concurrent STM imaging in this fashion minimises as much as possible any unintended STM tip induced manipulation. Molecular processes occur orders of magnitude faster than 10 ms, so our precautions do not preclude non-thermal events occurring but minimise their overall (time integrated) probability. Specifically we study the thermally induced adsorption changes of chlorobenzene, benzene and toluene (hereafter collectively referred to as 'aromatics') on the Si(1 1 1)-7×7 surface between room temperature and 47 °C. Large-scale time-lapse imaging allows us to measure the site-specific chemisorbed and physisorbed properties of these molecules on the Si(1 1 1)-7×7 surface. Our results not only catalogue the site-specific rates, but also indicate that the distribution of molecules between possible binding sites and their thermally induced dynamics is due to a combination of site-specific rates for a chemisorption to physisorption transition and the different site-specific rates for the reverse transition back to the chemisorbed state or escape to the gas phase.

2. Experimental

Time-lapse imaging of benzene and toluene was performed with a room temperature Omicron STM1 controlled by an RHK SPM-1000 in a UHV chamber at base pressure 2 × 10^{-10} Torr. Images were recorded at constant current mode under passive imaging parameters +1 V, 100 pA, which have been shown not to enhance or otherwise alter the thermal dynamics [13]. Si(1 1 1) samples were cut from 1–50 Ω cm n-type phosphorous doped wafers (Goodfellow SI2011/5). The Si(1 1 1)-7×7 reconstructed surface was generated by baking newly cut Si(1 1 1) crystals via direct current heating at 650 °C overnight, before repeated flashing to 1200 °C for 20 s to remove the SiO_2. A final flash followed immediately by a slow anneal from 960 °C to room temperature generated near pristine Si(1 1 1)-7×7 surfaces. The cleaning process was automated with excellent reproducibility, typically finding on average 0.002 contaminant 'black-spots' per Si adatom. Chlorobenzene, benzene and toluene (Sigma Aldrich) were purified by repeated freeze-pump-thaw cycles and monitored by mass-spectrometry. Variable temperature experiments for chlorobenzene on Si(1 1 1)-7×7 were done with an RHK-400 STM at base pressure 6 × 10^{-11} Torr. Tungsten STM tips were etched using the drop-off technique in 2M NaOH solution with a cathode bias of 9 V and subsequently annealed in vacuum to remove any oxide layer. Molecules were introduced to the UHV chamber via a computer controlled leak-valve, dosing at around 10^{-9} Torr to a coverage of ∼2 molecules per unit cell. Once dosed the sample was transferred into the STM and its surface was resolved within a few minutes.

3. Results and discussion

3.1. Adsorption geometry

Figure 1(*a*) shows an empty states STM image of the Si(1 1 1)-7×7 surface with the location of all 12 adatoms and 6 restatoms within a single unit cell indicated. Figure 1(*b*) shows a

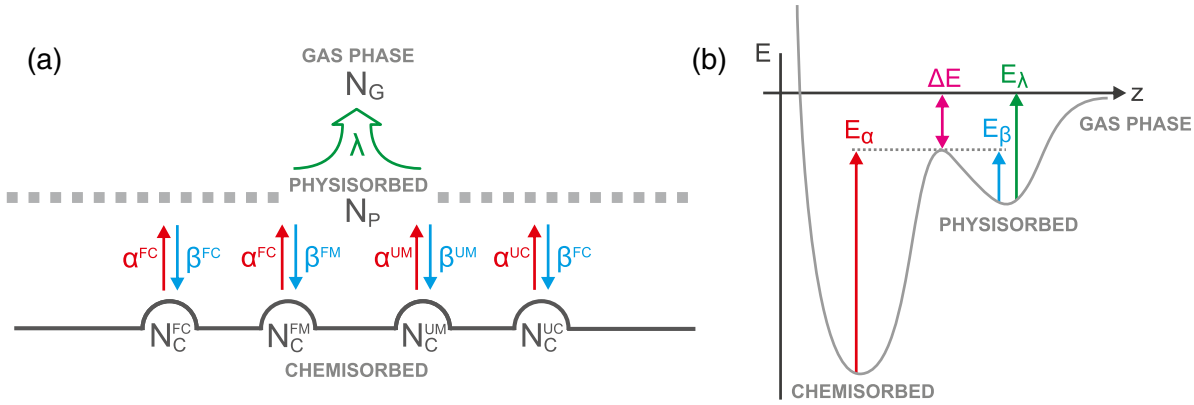

Figure 2. (*a*) Diagram displaying a model for the transition rates and populations of the four distinct surface chemisorbed sites, the physisorbed state and the gas phase (see main text for details). (*b*) Schematic diagram of the potential energy landscape of an aromatic molecule.

filled states image displaying the STM signature of the two distinct halves of the unit cell—the faulted half of the unit cell images more brightly than the unfaulted. The adsorption of chlorobenzene, benzene and toluene on the Si(1 1 1)-7×7 surface has been actively studied by many experimental and theoretical techniques [14–21]. These aromatic molecules chemisorb on the Si(1 1 1)-7×7 surface at room temperature and are imaged as 'missing' Si adatom features (i.e. black spots) in STM [14, 15]. Each molecule forms a pair of covalent bonds to two silicon atoms, one to a silicon adatom and one to a silicon restatom, so called di-σ bonding [20]. There are therefore four distinct binding configurations of aromatic molecules on the Si(1 1 1)-7×7 surface related to the type of adatom that the molecule binds to: faulted corner (FC), faulted middle (FM), unfaulted corner (UC) and unfaulted middle (UM). Within the faulted, or unfaulted, half of the unit cell the restatoms are identical. For a full description and STM image gallery of all possible binding sites with multiple molecules per unit cell please see [15].

The di-σ bonding configuration involves carbon atoms on opposite sides of the carbon ring. For benzene there is only one such distinct configuration for any adatom-restatom pair. For chlorobenzene and toluene there are several possible configurations dependent on the location of the chlorine or methyl group with respect to the carbon–silicon bonds. Theoretical and experimental results indicate that the lowest energy state is a 2–5 di-σ configuration [19, 20]. In our experiments we are insensitive to this fine detail and only record the presence of a molecule at an adatom site. On one occasion we have imaged chlorobenzene with high-resolution and observed an asperity in the image at the predicted location of the chlorine side group. Such intra-molecular resolution relies on a particular STM tip apex and typically at low temperatures such apices are created by the pick-up of an adsorbate. At room temperature such well defined apices are too unstable to allow prolonged (or even reproducible) imaging.

3.2. Adsorption potential energy landscape

Theoretical and experimental studies have explicitly observed that aromatic molecules chemisorb on the Si(1 1 1)-7×7 surface through a short-lived physisorbed precursor state. While in the precursor state a molecule may laterally explore the surface [14, 19, 22]. Even at low temperatures, e.g. 77 K, where molecules can be trapped in the physisorbed state, they cannot be reliably captured via STM as they are still able to diffuse across the surface [23]. At room temperature the physisorbed state is too short lived to appear in an STM image; from [24] we estimate the life time for physisorbed benzene on Si(1 1 1)-7×7 to be ∼1 μs. Instead, we image here the outcome of a molecule leaving its chemisorbed state, transiting through the physisorbed state, and either finding a chemisorption site (creating a new black spot) or leaving the surface entirely. Figures 1(*c*)–(*e*) present a short series of high resolution time-lapse STM images. Between image (*c*) and (*d*) the marked toluene molecule changes its binding site within the unit cell, and between (*d*) and (*e*) it disappears completely (desorbs).

Figure 2(*a*) shows a schematic model for the various processes that a molecule can undergo. From the four distinct chemisorbed sites the molecule can enter a common physisorbed state with rate constant α^x, where x indicates the FC, FM, UC, or UM site. In figure 2(*b*) we show a corresponding schematic of the potential energy curve with the energy barrier between the chemisorbed state and the transition state as E_α. From the physisorbed state a molecule can re-attach to the surface with site-specific rate β^x or desorb completely into the gas phase with rate λ, again the corresponding energies are indicated in the potential schematic of figure 2(*b*). In line with previous experimental and theoretical studies [14, 22, 23, 25] we do not include a directed chemisorbed-to-chemisorbed diffusive pathway, all diffusion occurs via the physisorbed state.

3.3. The chemisorbed state

We write the site-specific rate of change of the number of chemisorbed molecules, N_C^x, as the first order rate equation

$$\frac{dN_C^x}{dt} = -\alpha^x N_C^x. \quad (1)$$

Integration gives

$$\frac{N_C^x(t)}{N_C^x(0)} = \exp\left(-\alpha^x t\right). \quad (2)$$

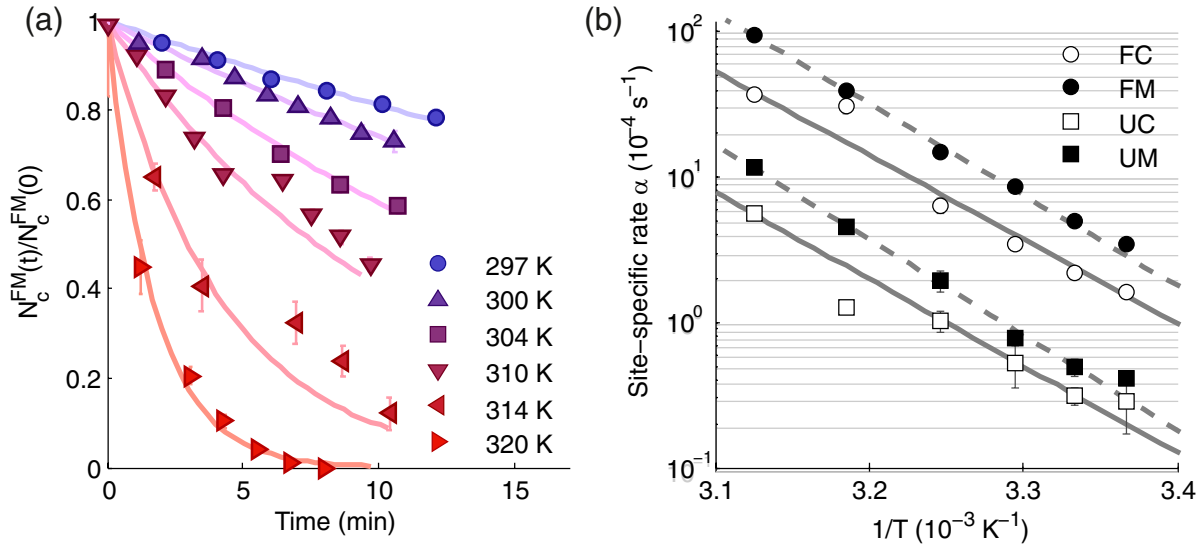

Figure 3. Site-specific chemisorbed to physisorbed transitions. (*a*) The time dependence of the fraction of chlorobenzene molecules at the faulted middle (FM) sites retaining their original position, $N_C^{FM}(t)/N_C^{FM}(0)$, as a function of temperature. (*b*) Arrhenius plot and best fits, for all four sites, for the rate of transition from chemisorbed to physisorbed states.

Table 1. The site-specific chemisorbed to physisorbed rates, α^x, for chlorobenzene, benzene and toluene. For chlorobenzene the pre-factors, A_α^x , and energy barriers, E_α^x, determined by Arrhenius fits of figure 3 are given.

	α^x (10^{-4} s^{-1})	A_α^x (s^{-1})	E_α^x (eV)	α^x (10^{-4})	α^x (10^{-4})
Site	Chlorobenzene			Benzene	Toluene
FC	1.64 ± 0.07	$10^{17.0\pm4.7}$	1.23 ± 0.13	10.32 ± 0.25	5.55 ± 0.37
FM	3.49 ± 0.19	$10^{16.6\pm1.3}$	1.19 ± 0.03	8.98 ± 0.20	8.41 ± 0.50
UC	0.29 ± 0.12	$10^{12.6\pm4.8}$	1.01 ± 0.13	2.09 ± 0.15	1.39 ± 0.08
UM	0.41 ± 0.02	$10^{16.6\pm2.5}$	1.24 ± 0.07	1.53 ± 0.12	0.75 ± 0.04

We measure the site-specific population, $N_C^x(t)$, by tracking every chemisorbed molecule in the initial image of a time-lapse series until it has moved from its site or the time-lapse series has ended (typically 10 sequential images). If a previously empty adatom site gains a chemisorbed molecule we follow that 'new' molecule until it has moved or the end the time-lapse series has ended. Hence we probe only the rate of removal (α^x) from each site. We are, however, insensitive to those events where a site has one molecule leave, and, before the next image, has another (or the same) molecule attach. Given the reasonably low coverage used (~2 molecules per unit cell) and the corresponding large number of possible binding sites we assume that this outcome has a minor effect on our results.

Figure 3(*a*) shows the measured time-dependent population $[N_C^{FM}(t)/N_C^{FM}(0)]$ for chlorobenzene molecules at at faulted middle (FM) sites at six temperatures from 297 K to 320 K. From this data we extract the site specific chemisorbed to physisorbed rate α^{FC}. Figure 3(*b*) presents an Arrhenius plot of these α rates for each of the four sites and associated best fits. Molecules attached to the faulted half have higher chemisorbed to physisorbed rates than those on the unfaulted half, middle sites have higher rates than corner sites. Thus we find for chlorobenzene $\alpha^{FM} > \alpha^{FC} \gg \alpha^{UM} > \alpha^{UC}$ at all temperatures.

Table 1 presents the Arrhenius pre-factors and energy barriers between chemisorbed and physisorbed states for each chemisorbed site for chlorobenzene, extracted from figure 3(*b*). Given the uncertainty in the parameters it is unclear whether the main influence on the rate of chemisorbed to physisorbed transition is the pre-factor or the energy barrier. Given that the geometry of faulted and unfaulted halves of the Si(1 1 1)-7×7 unit cell differ only in the 3rd layer of silicon atoms, it is reasonable to assume the local geometric environment of a molecule bonded to a faulted middle atom is near identical to that bonded to an unfaulted middle adatom. We find that we have the lowest uncertainty (best data) for the middle bonding molecules and that the pre-factors $A_\alpha^{FM} = A_\alpha^{UM}$ within error. The mean prefactor, as expected, is $10^{15.7\pm3.9} \approx 10^{16}$ s^{-1}, demonstrative of the molecule acquiring two-dimensional mobility as it leaves the immobile chemisorbed state [26]. What is different between the sites is the energy barriers, 0.05 eV higher on the unfaulted site than the faulted site. We would expect a similar analysis for corner bonded molecule, but with the larger experimental uncertainties for the rates and Arrhenius parameters a similar argument cannot be neither sustained nor disproved.

The measured site-specific rates for benzene and toluene at room temperature are also given in table 1. Overall benzene exhibits the highest rates of the three aromatics, chlorobenzene

the lowest. Applying the same pre-factors as measured for chlorobenzene, the measured difference in rates corresponds to a on average reduced (relative to chlorobenzene) chemisorbed to physisorbed energy barrier for benzene of 65 meV and toluene of 40 meV.

Unambiguously differentiating between pre-factors and energy barriers would require measurement across a larger temperature window. But even at 289 K (16 °C) the rates are so low that we see little measurable change across a 35 min experiment. The disadvantage of such slow rates is that any measured change has more chance of being induced, however unlikely, by some tip influence, or even created by the steady accumulation of surface contamination. At temperatures higher than 323 K (50 °C) the rates are high enough that it is difficult to gather a significant set of time-lapse images for analysis.

3.4. The physisorbed state

The physisorbed state of aromatic molecules on Si(1 1 1)-7×7 is too short lived at room temperature to resolve in an STM image [23]. However, we can observe the fate of a molecule that transits through the physisorbed state, finishing up as either chemisorbed at a new site on the surface, or having escaped into the gas phase. Between two consecutive time-lapse images the total drop in the number of chemisorbed molecules is equal to N_G, the number of molecules that leave the surface and enter the gas phase. Furthermore, comparing the atomic locations of all the molecules in two consecutive images we can identify the number of sites, initially empty, that acquire a chemisorbed molecule. We denote this as $N_C'^x$, where the prime indicates that this is the number of 'new' sites which gain a chemisorbed molecule (as opposed to the total number of sites that have a chemisorbed molecule). In this fashion we are able to compare the alternate outcomes of transiting through a physisorbed state. We acknowledge that any molecules that leave the scan field via diffusion between images would be mistakenly counted as undergoing desorption than diffusion (increasing N_G over $N_C'^x$). Given a scan size of 60 nm and diffusive step size of 2.3 nm [14], a simple calculation that gives molecules at the perimeter of the scan a 25% chance of leaving the field (via the closest edge), 3.6% of active molecules would leave the field. We can build a more sophisticated computational model of molecules on the Si(1 1 1)-7×7 surface: at a coverage of 2 molecules per unit cell, molecules diffuse to a random available site within 2.3 nm. Less than 2% of active molecules will leave the scan field. Given that this is an order of magnitude less than the fraction of molecules that are active, we consider this effect to be negligible.

If we consider the schematic of figure 2(*a*), the rate of change of N_G is simply related to the population of physisorbed molecules, N_p, and the rate constant, λ, by the 1st order rate equation $dN_G/dt = \lambda N_p$. Similarly the rate of change of 'new' chemisorbed sites will be $dN_C'^x/dt = \beta^x N_p$. Without direct time-resolved measurement of the physisorbed population we cannot directly solve these. However, the ratio of these rates yields

$$\frac{dN_C'^x}{dN_G} = \frac{\beta^x}{\lambda}. \tag{3}$$

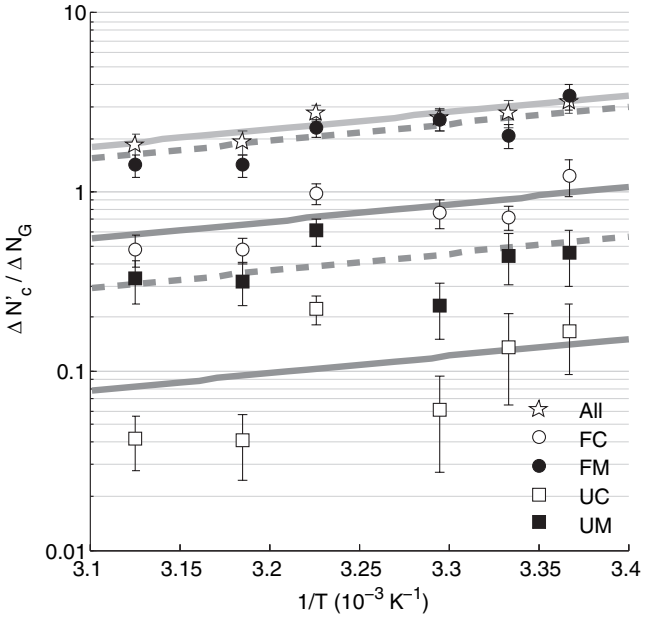

Figure 4. Arrhenuis plot and fits of the site-specific ratio $\Delta N_C'^x/\Delta N_G$ for chlorobenzene molecules on the Si(1 1 1)-7×7 surface (see main text for details and table 2 for Arrhenius parameters).

We relate this to the ratio of the measured number of new chemisorbed sites, $\Delta N_C'^x$, and the measured decrease in the overall population, ΔN_G, between two STM images. The ratio of rates β^x and λ can therefore be expressed in the normal Arrhenius manner yielding

$$\frac{\Delta N_C'^x}{\Delta N_G} = \frac{A_\beta^x}{A_\lambda} \exp\left(\Delta E/kT\right) \tag{4}$$

where ΔE is the absolute energy difference between the barrier to a transition between physisorbed to chemisorbed states and the barrier between the physisorbed and gas phases (see schematic in figures 2(*a*) and (*b*)).

For chlorobenzene, figure 4 shows an Arrhenius plot of the site-specific ratios $\Delta N_C'^x/\Delta N_G$ confirming their Arrhenius behaviour.

Inspection of the data shows that within the spread of the data points all four chemisorbed species have similar slopes, i.e. ΔE values. We therefore fit the full Arrhenius expression to the *total* number of new chemisorbed chlorobenzene molecules to find the site-average energy difference $\Delta E = 0.19 \pm 0.05$ eV with a corresponding site-average pre-factor ratio $A_\beta^{\text{mean}}/A_\lambda = (18.6 \pm 3.8) \times 10^{-4}$. Hence there is an energetic preference for molecules to chemisorb to the surface. However, chemisorbed molecules are immobile and experience significant steric hindrance. Entering the physisorbed state introduces translational freedom and a corresponding increase in pre-factor. The 10^3 increase in prefactor between physisorbed and gas phase is indicative of the molecule winning full rotational and translational freedom [26–28].

Since we have only room temperature measurements for benzene and toluene, we use the site-averaged pre-factor, A_β/A_λ, found for chlorobenzene to determine the energy

Table 2. The site-specific ratios A^x_β/A_λ for chlorobenzene, toluene, and benzene for transition rates between physisorbed state and chemisorbed state (A^x_β) and for transition between physisorbed state to the gas phase (A_λ).

	A^x_β/A_λ (10^{-4})		
Site	Chlorobenzene	Benzene	Toluene
FC	5.7 ± 0.6	6.4 ± 0.9	8.5 ± 1.7
FM	16.0 ± 1.2	14.0 ± 2.8	13.7 ± 2.8
UC	0.8 ± 0.2	1.0 ± 0.2	1.6 ± 0.3
UM	3.0 ± 0.4	1.4 ± 0.3	1.9 ± 0.4

difference ΔE for benzene (0.21 ± 0.05) eV, and for toluene (0.22 ± 0.05) eV. We note that, although within error, the rank order of energy differences ΔE, toluene 0.22 eV > benzene 0.21 eV > chlorobenzene 0.19 eV, follows the usual reactivity of substituted aromatic molecules based on their side group chemistry. Chlorobenzene is electron withdrawing, whereas methyl is electron donating. A detailed understanding of how these facts are related and manifest themselves on the potential energy landscape would require detailed theoretical study. The ~1.4 eV absorption energy found here agrees with a recent computational study [29].

Using the molecule specific values for ΔE we can extract the site-specific A^x_β/A_λ pre-factor ratios (see table 2) for all three molecules (the error in A^x_β/A_λ for cholorobenzene is the standard error from all temperature points, an average of 14%, and we assume a 20% error margin for benzene and toluene). For all three molecules the faulted half of the unit cell has a greater Arrhenius pre-factor ratio and, within the half-unit cell, middle sites have a higher factor than corners. The latter difference can partly be explained by the entropic differences in binding to a middle and corner adatoms: there are two possible configurations per middle adatom, whereas for corners there is only one restatom available. At low temperatures molecule have a long lifetime in the physisorbed state and can be imagined by STM (as smeared bright features) predominately at middle adatom sites, and occasionally at the faulted corner sites [21, 23, 30]. Presumably there are subtle variations in the energy of the physisorption well that dictate the time such mobile physisorbed molecules spend at a given site leading to the observed STM images and our Arrhenius pre-factor ratios.

3.5. Long-term population trends

To further test the proposed model, as depicted in figure 2(*a*), that describes the connections between the chemisorbed, physisorbed and gas phases, figure 5 shows the changing site-specific population of benzene molecules on Si(1 1 1)-7×7 over the course of several hours and compares with simple numerical simulations based on the rates measured in our 12 min duration time-lapse experiments. Can the PES parameters from our 12 min experiments describe the long time evolution of the system? Thirty STM images were taken over a 3 h period and, to reduce any possible tip influence and to average over any fluctuations in the various population from area to area, each image was taken at a new location. What is striking is that although the faulted half populations start out

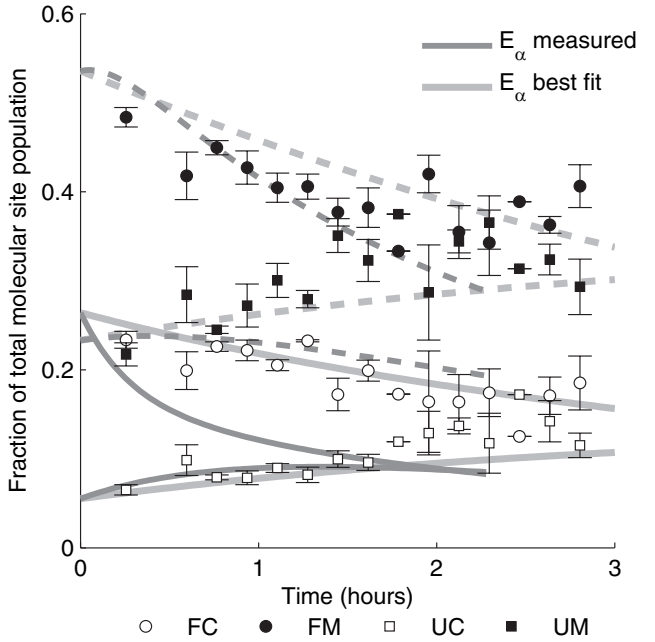

Figure 5. Long-term plot of the fractional site-specific coverage of benzene molecules on the Si(1 1 1)-7×7 surface at room temperature. Dark grey lines map the evolution based on our measured rates in tables 1 and 2. Light grey lines are given by a multi-parameter fitting routine based on the measured rates. See text for fitting parameters.

higher than the unfaulted, over time the unfaulted sites become populated by molecules originating from the faulted half.

During the initial dose all molecules must enter the physisorbed state from the gas-phase and subsequently chemisorb (or desorb). The initial site-specific populations should therefore reflect the competing rates out of the physisorbed state. Here these are reflected in the differing A^x_β/A_λ ratios of table 2. Both the initial populations and the pre-factor ratios for benzene follow the same ordering, FM > FC > UM > UC. Over time the higher rate constant of molecules at FM and FC sites to re-enter the physisorbed state empties those sites and redistributes molecules between all the sites according to the relative β^x values. Thus the overall populations of FM and FC molecules drop and, as a consequence, the populations of UM and UC sites increase. Since the rates of leaving these unfaulted sites are (relatively) low these sites act as 'sinks' for the molecules. The dark grey lines of figure 5 show the simulated long term evolution of the system using the site-specific rates and energy barriers derived above for benzene at $T = 293$ K.[3] There is agreement between the PES data and the long-term plot over the duration of a 12 min time-lapse. Beyond this point there is a divergence as

[3] The simulation uses the experimentally derived site-dependent rates for transport between the chemisorbed and physisorbed states. A distribution of chemisorbed molecules is initialised with relative populations defined by the relative size of the physisorbed to chemisorbed rates. The system then evolves, with a time step of 100 s, using the chemisorbed to physisorbed rates to generate a physisorbed population, and the return rates to redistribute the physisorbed molecules. Temperature controls the magnitude of the rates via the Arrhenius relation and is kept fixed throughout an experiment. To disentangle the physisorbed to chemisorbed and physisorbed to gas phase rates, we assume $A_\lambda = 10^{20}$.

the PES measured predicts a faster emptying of FC and UM sites than observed. Over 2 h there is still a good qualitative and quantitative agreement the PES data and the long term trends for FM and UC sites. Past 2 h there is further divergence, however allowing some degree of fitting to the raw data allows our model to map the full evolution of the system (light grey lines in figure 5). We find an excellent match to the full evolution of the system with a fit that keeps the site-specific prefactors fixed to those measured and $T = 293.3$ K, $E_\alpha^{\mathrm{FM}} = 1.17$ eV, $E_\alpha^{\mathrm{UC}} = 1.0$ eV and $E_\alpha^{\mathrm{UM}} = 1.25$ eV, within error of the measured barriers. Deviations at long terms may occur as more subtle effects may come into play, such as surface contamination buildup, a reduction in the overall benzene coverage and the blocking of certain diffusion pathways as some adsorption sites saturate. Further work with more sophisticated models could reveal more about surface transport in the long term.

Previously we reported the thermal rate of displacement (desorption and diffusion) of chlorobenzene on Si(1 1 1)-7×7 with a lower Arrhenius prefactor of $(10^{10.8\pm1.3})\,\mathrm{s}^{-1}$ and lower energy barrier of (0.84 ± 0.08) eV [13]. These values are quite different from the corresponding values present here in table 1. However the values of [13] were obtained without site-discrimination, each measured rate at a particular temperature was, in effect, a weighted average of the site-specific population. The long-time population of chlorobenzene molecules on Si(1 1 1)-7×7 follows a very similar trend as for benzene. Therefore at low temperature, where the relative populations reflects the physisorbed to chemisorbed rates, the FM and FC population are largest, thus biasing the mean rate. During our time-lapse measurements taken at higher temperatures, the site-specific population will significantly change, skewing the average towards the unfaulted molecules' properties. Hence an average over all sites does not accurately reflect the true underlying dynamics of the ground state molecule/surface system.

4. Conclusion

In summary we have presented a detailed time-lapse STM study of the site-specific dynamics of small aromatic organic molecules on the Si(1 1 1)-7×7 surface. By careful analysis we extract the Arrhenius factors for both transition from the chemisorbed state to the physisorbed state, and the (relative) Arrhenius factors for transition out of the physisorbed state back to the chemisorbed state or exit into the gas phase. Our results demonstrate the power of such atomic resolution imaging but also highlight a number of limitations. This is especially true where an experimental measurement cannot discriminate against several pathways that have markedly different kinetic properties but lead to the same measured result.

Acknowledgments

PAS gratefully acknowledges support from the EPSRC grant EP/K00137X/1. DL was funded by an EPSRC DTA studentship and SS acknowledges the award of a Thailand Higher Educational Strategic Scholarship. REP acknowledges support by the EPSRC.

References

[1] Ryan P M, Livadaru L, DiLabio G A and Wolkow R A 2012 *J. Am. Chem. Soc.* **134** 12054–63
[2] Salfi J, Mol J A, Rahman R, Klimeck G, Simmons M Y, Hollenberg L C L and Rogge S 2014 *Nat. Mater.* **13** 605–10
[3] Bellec A, Chaput L, Dujardin G, Riedel D, Stauffer L and Sonnet P 2013 *Phys. Rev.* B **88** 241406
[4] Renaud N, Hliwa M and Joachim C 2012 *Unimolecular and Supramolecular Electronics II: Chemistry and Physics Meet at Metal-Molecule Interfaces* (*Topics in Current Chemistry*) vol 313, ed R M Metzger (New York: Springer) pp 217–68
[5] Hla S W 2014 *Rep. Prog. Phys.* **77** 056502
[6] Morgenstern K, Lorente N and Rieder K H 2013 *Phys. Status Solidi* B **250** 1671–751
[7] Sloan P A and Palmer R E 2005 *Nature* **434** 367–71
[8] Kreuzer H J, Payne S H, Drozdowski A and Menzel D 1999 *J. Chem. Phys.* **110** 6982–99
[9] Kang H and Weinberg W 1994 *Surf. Sci.* **299–300** 755–68
[10] Lombardo S J and Bell A T 1991 *Surf. Sci. Rep.* **13** 3–72
[11] Sloan P A 2010 *J. Phys.: Condens. Matter* **22** 264001
[12] Sakulsermsuk S, Palmer R E and Sloan P A 2012 *J. Phys.: Condens. Matter* **24** 394014
[13] Sakulsermsuk S, Sloan P A and Palmer R E 2010 *ACS Nano* **4** 7344–8
[14] Wolkow R A and Moffatt D J 1995 *J. Chem. Phys.* **103** 10696
[15] Sloan P A and Palmer R E 2006 *J. Phys.: Condens. Matter* **18** S1873–85
[16] Taguchi Y, Fujisawa M and Nishijima M 1991 *Chem. Phys. Lett.* **178** 363–8
[17] Jiang G, Polanyi J C and Rogers D 2003 *Surf. Sci.* **544** 147–61
[18] Tomimoto H, Takehara T, Fukawa K, Sumii R, Sekitani T and Tanaka K 2003 *Surf. Sci.* **526** 341–50
[19] Tomimoto H, Sekitani T, Sumii R, Oda Sako E, Wada S I and Tanaka K 2004 *Surf. Sci.* **566–8** 664–70
[20] Cao Y, Deng J F and Xu G Q 2000 *J. Chem. Phys.* **112** 4759
[21] Dobrin S *et al* 2007 *Nanotechnology* **18** 044012
[22] Weymouth A J, Miwa R H, Srivastava G P and McLean A B 2010 *Phys. Status Solidi* C **7** 240–3
[23] Brown D E 1998 *Science* **279** 542–4
[24] Dobrin S, Rajamma Harikumar K and Polanyi J C 2004 *Surf. Sci.* **561** 11–24
[25] Yong K S, Yang S W, Zhang Y P, Wu P and Xu G Q 2008 *Langmuir* **24** 3289–93
[26] Thomas J and Thomas W 1996 *Principles and Practice of Heterogeneous Catalysis* (New York: VCH)
[27] Lüth H 2010 *Solid Surfaces, Interfaces and Thin Films* (*Graduate Texts in Physics*) (New York: Springer)
[28] Ibach H, Erley W and Wagner H 1980 *Surf. Sci.* **92** 29–42
[29] Utecht M, Pan T, Klamroth T and Palmer R E 2014 *J. Phys. Chem.* A **118** 6699–704
[30] Lu X, Polanyi J C and Yang J S Y 2006 *Nano Lett.* **6** 809–14